IEEE Access
Multidisciplinary ⋮ Rapid Review ⋮ Open Access Journal

Received February 18, 2022, accepted March 22, 2022, date of publication March 25, 2022, date of current version March 30, 2022.

Digital Object Identifier 10.1109/ACCESS.2022.3162415

Torsional Vibration Suppression in Railway Traction Drives

AHMED FATHY ABOUZEID[1,2], (Member, IEEE), JUAN M. GUERRERO[1], (Senior Member, IEEE), IBAN VICENTE-MAKAZAGA[3], IKER MUNIATEGUI-ASPIAZU[3], AITOR ENDEMAÑO-ISASI[3], AND FERNANDO BRIZ[1], (Senior Member, IEEE)

[1]Department of Electrical, Electronic and Computer Engineering, University of Oviedo, 33003 Oviedo, Spain
[2]Department of Electrical Engineering, Port Said University, Port Said 42526, Egypt
[3]Department of Traction Systems, Ingeteam Power Technology, 48170 Zamudio, Spain

Corresponding author: Ahmed Fathy Abouzeid (abouzeidahmed@uniovi.es)

This work was supported in part by the European Commission H2020 under Grant UE-18-POWER2POWER-826417; in part by the Spanish Ministry of Science, Innovation and Universities under Grant MCIU-19-PCI2019-103490; and in part by the Government of Asturias under Project AYUD/2021/50988. The work of Ahmed Fathy Abouzeid was supported in part by the Scholarship from the Ministry of Higher Education and Scientific Research of Egypt.

ABSTRACT Torsional vibrations phenomena are self-excited vibrations that occur in the wheelset of railway powertrains due to the counter-phase oscillation of both wheels. Long-lasting events of this type may lead to the catastrophic failures. Therefore, torsional vibration suppression and mitigation methods have drawn significant attention from the railway industry in the recent few years. Conventional vibration suppression methods reduce motor torque once the oscillation is detected. However, this can result in trip delays. Design of methods which do not compromise the traction capability is challenging. This paper proposes a novel torsional vibration suppression method using a Proportional-Resonant (PR) controller. The proposed method is insensitive to mechanical drive-train parameter variation neither requires adding new sensors to the wheelset. The method requires previous knowledge of the natural frequency of the wheelset torsional mode but this significantly reduces the implementation complexity suffered by other anti-vibration methods. Furthermore, the method will be shown to provide reduced sensitivity to slip velocities and wheel-rail conditions.

INDEX TERMS Railway traction drives, torsional vibrations, slip-stick phenomenon, slip control, field-oriented control, proportional-resonant controller.

I. INTRODUCTION

Derailment is one of the serious problems that should be avoided in railways for ensuring passengers' safety and reducing maintenance costs. Derailment occurs when the train vehicle comes off the track (i.e. the rail) which could lead to major accidents and collisions [1]. Failure in the mechanical components of the vehicle, track geometry defect (due to excessive wear of wheels or rails), and wheel-rail interaction such as excessive creepage are the most significant reasons for the train vehicle derailment [2], [3]. Therefore, many efforts have been devoted to limiting the creep (i.e. slip) between the wheel and the rail [4]–[6].

A certain amount of slip between wheel and rail is needed to increase the tractive force generated by the traction motor to the rail. Traditional creep controllers, also known as re-adhesion controllers, avoid slippage (i.e. the condition when the wheel-rail slip velocity dramatically increases) by limiting the slip velocity within a predefined threshold [7], [8]. They can be divided into two types:

1) Direct methods: they compare either the wheel circumference slip velocity or the wheel acceleration with a predefined threshold [9]–[11]. The threshold is chosen based on field-tests and trains' driver experience [12], [13]. The main drawback of the direct methods is that the re-adhesion controller cannot optimally utilize the adhesion in different rail surface conditions.
2) Indirect methods: they are intended for rolling stocks where multiple motors are fed from the same inverter. It is assumed that the speed of all paralleled motors is not measured [14], some form of sensorless vector control is therefore normally used. Slip is detected in

The associate editor coordinating the review of this manuscript and approving it for publication was Zhuang Xu.

this case from unbalances in the current consumed by the paralleled motors. An obvious limitation of this method is that it can only be used when the traction converter feeds multiple motors.

Modern high-speed railway traction drives are often equipped with slip controllers aimed to operate at the possible maximum adhesion point while preventing slippage. Slip controllers make use of the adhesion-slip characteristic curve; reported approaches include:

1) Direct adaptation of the torque command using an adhesion force controller. Maximum adhesion occurs when the adhesion force gradient equals to zero (i.e. at the peak of the adhesion-slip curve). Steepest gradient method or Proportional-Integral (PI) controllers aimed to keep the adhesion slope equal to zero are commonly used for this purpose. [15]–[20].
2) Regulation of the slip velocity using an additional speed controller [21]–[23]. In this case, the slip velocity reference is increased progressively in small steps, the commanded torque being monitored. When a slip increase results in a decrease in the commanded torque, it is considered that maximum adhesion has been surpassed.

Finding the optimal slip velocity is a challenging task due to the high unpredictability of adhesion-slip phenomena and the subsequent uncertainty in the estimations. Several approaches have been proposed for this purpose, including: perturb and observe methods (P&O) [24], [25]; recursive least squares searching [26]–[28]. Model predictive control and particle swarm intelligence methods are also be found in [29], [30]. However, these searching algorithms increase the complexity of the control and their implementation in real trains has not been reported in the literature.

While slip controllers enhanced with maximum adhesion tracking increase the utilization of tractive force for high-performance locomotives, they can potentially enter the unstable adhesion region during the searching. As a result, oscillations can arise in the torsional elements of the locomotives power train [31]. These oscillations can also be provoked by slip-stick phenomenon due to changes in the adhesion condition and track irregularities. The most severe oscillation occurs when both wheels of the locomotive oscillate in counter-phase, which is sometimes referred as slip-stick vibration. Such vibrations add more stress on the press-fit joints of the wheelset axle, and could lead to their failure and, as a consequence, to the derailment of the locomotive.

Excitation of torsional resonances by the torque ripple and the interaction between the electric and mechanical elements are the main source of such vibrations [32]. Torsional vibrations in mechanical systems fed from electrical drives can be either passively or actively damped [33]. Passive cancellation can be implemented using Infinite Impulse Response (IIR) notch filters. The filter is designed to remove dangerous oscillations from the torque command [34], avoiding their propagation to the mechanical system. However, notch filters might fail to suppress completely the resonant frequency due to the output delays and the uncertainty in the location of the resonance poles and zeros due to changes of the inertia constant of the mechanical system. A Finite Impulse Response (FIR) notch filter compensator can be used instead [35], taking advantage of FIR systems intrinsic stability and linear phase shift [36], [37]. Excitation of resonant modes can be also avoided using an FIR compensator by halving the output of the speed controller and delaying one of the halves by half the resonance period, later adding it to the non-modified half signal, which eventually cancels the oscillation [35]. The limitation of this approach relies on torque control transient response and the noise in the feedback speed sensor.

Active damping of torsional vibration can be achieved by using state feedback compensation where the torque command can be adapted through the feedback signals of torque control loop, speed control loop, or both [38]. Thus, all system poles can be placed at the desired location by choosing the appropriate feedback gains [39], [40]. Usually, these methods require an estimator or observer for non-measurable states [40], [41]. Moreover, advanced control techniques using Linear Quadratic Regulator (LQR), Linear Quadratic Gaussian (LQC), and H_∞ have been also proposed in [42]–[44]. However, these methods are highly sensitive to system parameters, meaning that for successful implementation they might need to be combined with parameter identification methods. Furthermore, the aforementioned torsional vibration methods use simplified mechanical models, ignoring therefore system dynamics, sensor noise, and other unexpected disturbances, which can be highly relevant in railways due to wheel-rail slippage phenomena.

Analysis and modeling of self-excited torsional vibrations phenomena in railways has been discussed in [45]–[48]. In [49], an indirect passive anti-vibration control is proposed. Torsional vibrations are extracted from the estimated dynamic of the wheelset axle. If they exceed a predefined limit, the control reduces the torque command. The effectiveness of this method strongly relies on quick detection of slip. While simple and therefore easy to implement, the main shortcomings of this method are a decrease of traction capability during the oscillation mitigation process, and the need for additional wheel sensors, which increase the cost and require the reconfiguration of existing locomotives in service. In [50], a state-space active anti-vibration control integrated with a slip re-adhesion control is proposed. This control strategy was capable of damping slip-stick vibrations up to a certain negative gradient of the adhesion force characteristic. The method was further improved by adding a virtual absorber at the indirectly driven wheel to suppress the torsional vibrations [51]. Complete vibration damping at any negative value of adhesion force gradient and without losing the traction capability is feasible with the virtual damper approach. The drawbacks of this method are its complexity

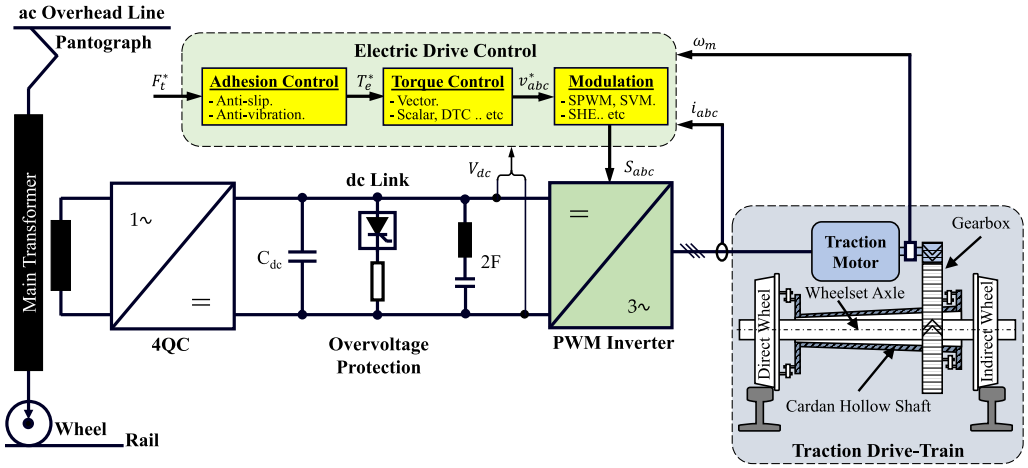

FIGURE 1. Schematic representation of a single-driven axle for a high-performance locomotive.

and the difficult tuning of the controller and the observer. Furthermore, natural frequencies identification is required to adapt the mechanical drive-train parameters to reflect variations due to wear and aging.

This paper proposes a torsional vibration suppression method using a resonant controller. The proposed method will be shown to be robust against changes in slip velocity and wheel-rail conditions. The paper is organized as follows. Section II describes the traction drive system for railways. Section III presents the detailed mechanical drive-train and locomotive model. The slip velocity control and the proposed vibration suppression method are addressed in IV. The proposed method is validated by simulation in section V. Finally, a summary of findings is provided in section VI.

II. SYSTEM DESCRIPTION

This section overviews the powertrain for high-performance locomotives (Fig. 1). The pantograph transfers the electrical power from the overhead line (ac or dc) to the locomotive. The ac transmission voltage can be 25 kV/50 Hz or 15 kV/16.7 Hz while the dc voltage can be 3 kV or 1.5 kV. For ac catenaries, the main transformer normally consists of a primary high-voltage winding with multiple secondary windings supplying both the traction converters and the auxiliary systems for heating, ventilation, and air conditioning (HVAC), lighting, etc.

A four-quadrant power converter (4QC) provides the dc-link voltage feeding the traction inverters, which are responsible for controlling the torque produced by motors according to the locomotive driver commands. Motor torque is transferred to the wheels through the mechanical drive-train, producing the traction force.

The electric drive control is responsible for achieving the traction force F_t^* commanded by the driver. As shown in Fig. 1, it consists of three main blocks: modulation, torque control, and adhesion control.

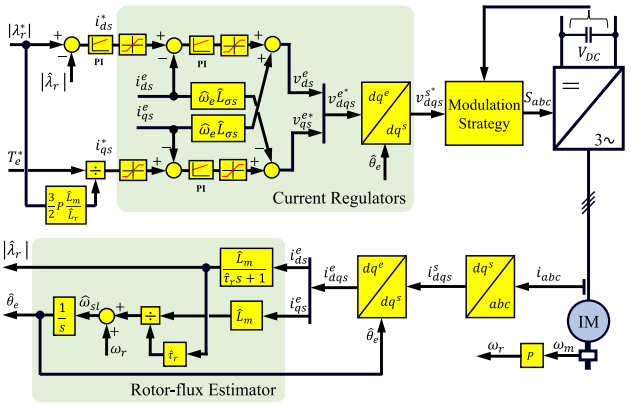

FIGURE 2. Rotor field-oriented control (RFOC) scheme.

A. TORQUE CONTROL AND MODULATION TECHNIQUE

Vector control schemes are preferred at low speed since they allow precise control of torque and flux, which is achieved employing high-performance current regulators. Typically rotor flux field-oriented control (RFOC) is used (see Fig. 2). The electromagnetic torque T_e using RFOC can be represented by (1). As observed from (1), torque can be controlled through the q-axis current i_{qs}^e; high bandwidth current regulators are used for this purpose.

$$T_e = \frac{3}{2} P \frac{L_m}{L_r} \lambda_r i_{qs}^e \tag{1}$$

where P is the number of pole-pairs; L_m, L_r are the magnetizing and rotor inductances respectively; λ_r is the rotor flux.

At low speeds with RFOC, the inverter usually operates with constant switching frequency using either carrier-based Pulse-Width Modulation (PWM) with triplen harmonic injection or Space Vector PWM. Both two-level and three-level neutral-point clamped voltage-source inverters (3L-NPC-VSI) using insulated-gate bipolar transistors (IGBTs)

are of common use for traction drive [52]. The 3L-NPC-VSI will be used in this paper.

For high-speed operation, the inverter often operates with low switching-to-fundamental frequency ratios and high modulation indexes, including full-wave. Due to this, synchronous modulation methods, including Selective Harmonic Elimination (SHE), combined with scalar control, are a common choice in this case [53].

The electric drive control strategy can play a major role in the implementation of torsional vibration cancellation. A key aspect to consider is the bandwidth of the torque control, ROFC being in general advantageous over scalar control methods in this regard. This issue is addressed in section V-B.

B. ADHESION CONTROL

This block is responsible for adjusting the traction force to the wheel-rail adhesion level to prevent the wheel from slipping out, especially during acceleration/deceleration of the locomotive or in the event of sudden changes of the wheel-rail contact conditions. Recently with the rising awareness of torsional vibrations and their side effects on the wheelset axle, the adhesion control block has been enhanced with an additional anti-vibration control strategy. The details on the slip and anti-vibration control method will be discussed in section IV.

III. MECHANICAL DRIVE-TRAIN MODEL

This section discusses the mechanical model of the drive-train system. The hollow shaft drive-train of the German class 120 locomotive has been selected for the analysis [54], [55].

A. MATHEMATICAL MODEL

The traction drive-train consists of six rotational masses that are connected by torsional elements in the series structure as follows (see Fig. 3).

- The induction motor generates a drive torque T_e transmitted through the coupling to the gearbox T_M.
- Then the torque exerted in the gearbox T_{MG} is transmitted to the direct-driven wheel T_{HD} through the cardan hollow shaft, where the total inertia of the hollow shaft including the braking discs and couplings is divided into two rotating masses connected by an elastic shaft. The received torque at the direct driven wheel follows the transmission sequence: 1) from the gearbox to the first half of hollow shaft (gear side) through a gear-hollow shaft coupling T_{GH}; 2) then to the second half of the hollow shaft (wheel side) via the elastic shaft T_{HW}; 3) afterward to the direct-driven wheel T_{HD} through the hollow shaft-wheel coupling.
- Finally, the torque is transmitted to the indirect-driven wheel via the wheelset axle T_{DI}.

The general motion equation is given by (2),

$$[J] \cdot [\ddot{\theta}] + [D] \cdot [\dot{\theta}] + [C] \cdot [\theta] = [T] \tag{2}$$

where J, D, and C are the inertia, damping ratio, and stiffness matrices, respectively. θ, $\dot{\theta}$ and $\ddot{\theta}$ are the rotational angle, its first and second derivatives matrices, respectively. T is the applied torque matrix.

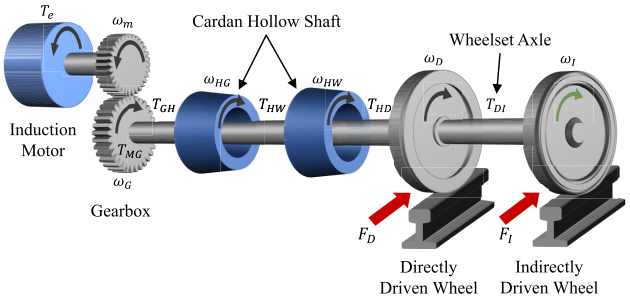

FIGURE 3. Six-inertia model of the mechanical traction drive-train. Torque transmission from motor to direct and indirect wheels are indicated by black and green arrows respectively; adhesion forces exerted on both wheels are indicated by red arrows.

Applying (2) to the drive-train in Fig. 3, the differential equations of the six-inertia model (3), as shown at the bottom of the next page, are obtained, where: j_M, j_G, j_{HG}, j_{HW}, j_D and j_I represent the inertia of the motor, the gear, the hollow-gear, the hollow-wheel, the direct and the indirect wheels respectively; d_{MG}, d_{GH}, d_{HW}, d_{HD}, and d_{DI}; c_{MG}, c_{GH}, c_{HW}, c_{HD}, and c_{DI} are the torsional damping and stiffness values of the motor to the gear, the gear to the hollow shaft, the hollow shaft gear side to the hollow shaft wheel side, the hollow shaft wheel side to the direct wheel and the direct to indirect wheels respectively. T_M, T_D, and T_I are the motor torque and the traction torques applied to the direct and indirect wheels respectively. Note that all values in (3) are referred to the wheelset side of the drive-train, with R_g being the gear ratio.

B. SIMULATION MODEL

Applying Laplace transformation to (3), the drive-train block diagram Fig. 4 is obtained. The transmitted traction forces in the wheel-rail contact point are calculated from (4) where r_w, $\mu_{D,I}$ and $T_{D,I}$ are the wheel radius, adhesion coefficient and torque on each wheel, respectively; m_l, N_m, g are the locomotive mass, the total number of motors and the gravity constant, respectively.

$$T_{D,I} = r_w \cdot F_{D,I} = r_w \cdot \mu_{D,I} \cdot \frac{m_l \cdot g}{2 \cdot N_m} \tag{4}$$

The adhesion characteristics for different wheel-rail conditions (dry, wet, …etc.) are calculated offline and stored in a look-up table [7]. Finally, the train speed v_{train} is obtained as shown in Fig. 5, where m_t is the total mass of the train, F_{res} is the resistive force due to the air (K_{air}) and rolling (K_{roll}) resistances [55]. Forces due to track grading are not shown in this figure. It is noted that the vehicle model in Fig. 5 assumes that all powered axles transmit the same traction force.

C. MODAL ANALYSIS

Modal analysis is a useful tool to identify the most stressed elements of the mechanical drive-train from vibration characteristics, i.e. natural frequencies and mode shapes. Natural frequencies, also referred to as resonance frequencies,

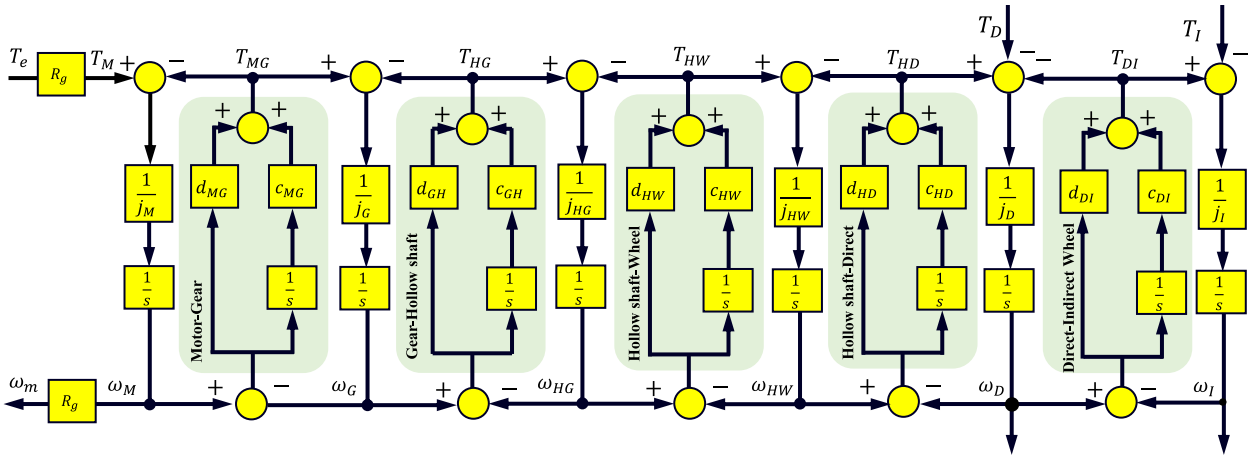

FIGURE 4. Block diagram of the six-inertia drive-train model.

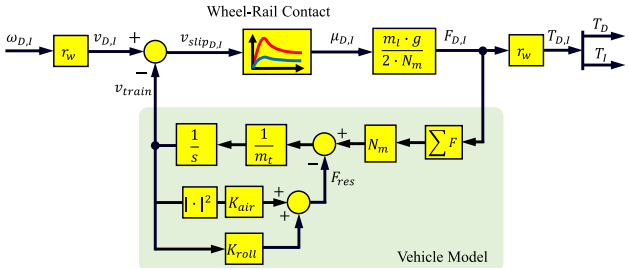

FIGURE 5. Block diagram of the wheel-rail contact model including the vehicle dynamics.

indicate the vibration modes of the elastic elements in the drive-train; mode shapes indicate the relative displacement between adjacent elements (inertias).

Drive-train natural frequencies and mode shapes can be obtained from the homogeneous equation (2) using (5), where λ, $[I]$ represent the eigenvalues (roots) of the system and the identity matrix respectively. It is noted that damping coefficients have been neglected, which corresponds to the worst-case scenario.

$$det\left(\lambda^2 \cdot [I] - [J]^{-1} \cdot [C]\right) = 0 \tag{5}$$

where eigenvalues represent the resonance frequencies of the mechanical system, eigenvectors represent the angle deviation and the direction of rotation for each inertia relative to adjacent inertias. Mode shape is a graphical representation that shows the angle deviation between the mechanical element at each resonance frequency (see Fig. 6). Eigenvalues and eigenvectors problems for the targeted drive-train model are obtained using MATLAB and normalized based on the maximum angle deviation found from all elements at each mode. For instance, in the second mode, the indirect wheel has the maximum angle deviation which is selected to be the base value for the rest of the elements. The six-inertia system consists of five torsional stiffness elements, producing five natural frequencies and mode shapes, in addition to one trivial mode as the discussed following (see Fig. 6):

$$\begin{bmatrix} j_M & 0 & 0 & 0 & 0 & 0 \\ 0 & j_G & 0 & 0 & 0 & 0 \\ 0 & 0 & j_{HG} & 0 & 0 & 0 \\ 0 & 0 & 0 & j_{HW} & 0 & 0 \\ 0 & 0 & 0 & 0 & j_D & 0 \\ 0 & 0 & 0 & 0 & 0 & j_I \end{bmatrix} \cdot \begin{bmatrix} \ddot{\theta_M} \\ \ddot{\theta_G} \\ \ddot{\theta_{HG}} \\ \ddot{\theta_{HW}} \\ \ddot{\theta_D} \\ \ddot{\theta_I} \end{bmatrix}$$
$$+ \begin{bmatrix} d_{MG} & -d_{MG} & 0 & 0 & 0 & 0 \\ d_{MG} & (d_{MG}+d_{GH}) & -d_{GH} & 0 & 0 & 0 \\ 0 & -d_{GH} & (d_{GH}+d_{HW}) & -d_{HW} & 0 & 0 \\ 0 & 0 & -d_{HW} & (d_{HW}+d_{HD}) & -d_{HD} & 0 \\ 0 & 0 & 0 & -d_{HD} & (d_{HD}+d_{DI}) & -d_{DI} \\ 0 & 0 & 0 & 0 & -d_{DI} & d_{DI} \end{bmatrix} \cdot \begin{bmatrix} \dot{\theta_M} \\ \dot{\theta_G} \\ \dot{\theta_{HG}} \\ \dot{\theta_{HW}} \\ \dot{\theta_D} \\ \dot{\theta_I} \end{bmatrix}$$
$$+ \begin{bmatrix} c_{MG} & -c_{MG} & 0 & 0 & 0 & 0 \\ c_{MG} & (c_{MG}+c_{GH}) & -c_{GH} & 0 & 0 & 0 \\ 0 & -c_{GH} & (c_{GH}+c_{HW}) & -c_{HW} & 0 & 0 \\ 0 & 0 & -c_{HW} & (c_{HW}+c_{HD}) & -c_{HD} & 0 \\ 0 & 0 & 0 & -c_{HD} & (c_{HD}+c_{DI}) & -c_{DI} \\ 0 & 0 & 0 & 0 & -c_{DI} & c_{DI} \end{bmatrix} \cdot \begin{bmatrix} \theta_M \\ \theta_G \\ \theta_{HG} \\ \theta_{HW} \\ \theta_D \\ \theta_I \end{bmatrix} = \begin{bmatrix} T_M \\ 0 \\ 0 \\ 0 \\ -T_D \\ -T_I \end{bmatrix} \tag{3}$$

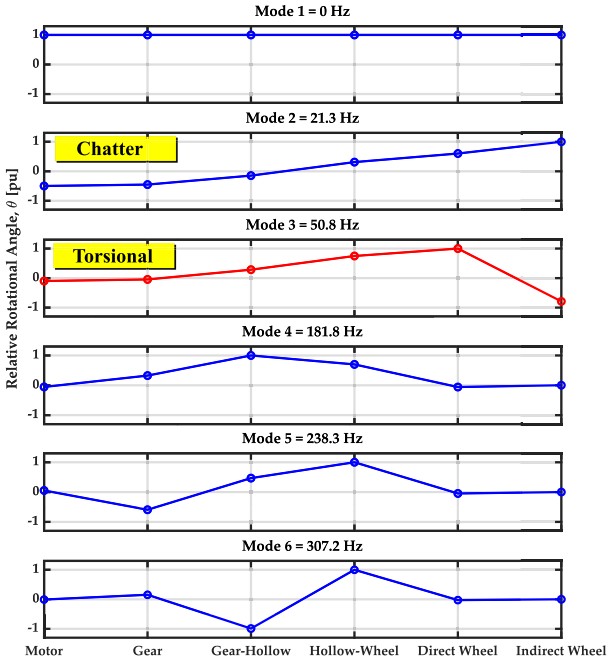

FIGURE 6. Mode shapes of the six-inertia model.

- First mode shape occurs at 0 Hz and is due to the rigid body motion.
- Second mode shape (i.e. the first vibration mode) is located at 21.3 Hz and occurs when the whole wheelset oscillates against the motor. This vibration mode can be totally damped using a proper speed controller [54].
- Third mode shape reveals the second vibration mode at 50.8 Hz, which occurs when direct and indirect wheels oscillate in the counter phase, twisting the wheelset axle. It can be noticed that this vibration mode can have a reduced impact on the motor. Detectability of the second vibration by motor control will play a key role for active damping methods, use of speed/position sensors directly attached to the wheels might be required otherwise.
- The remaining mode shapes at higher frequencies have less influence on the traction motor and the wheelset, hence, they are normally neglected [51].

IV. WHEEL-RAIL SLIP CONTROL AND PROPOSED TORSIONAL VIBRATIONS SUPPRESSION

This section first discusses slip-stick phenomenon, its effect on initiating the torsional vibrations and the available methods for their suppression. A new method, which is the main contribution of this paper, is proposed in Section IV-C.

A. SLIP CONTROL AND VIBRATION EXCITATION

As mentioned in section II-B, the traction force is regulated by adapting the slip velocity between the wheel and the rail. The slip velocity command can be modified to maximize the adhesion level with different operating conditions or simply kept at a certain value that does not exert much wear on the rail. The slip velocity is calculated from the motor speed and the estimated train velocity. Either P or PI controllers can be used to track the commanded slip velocity. The block diagram of the traction drive control is shown in Fig. 7.

Slip controller tuning is not trivial, as mechanical system dynamics depend on the non-linear wheel-rail contact characteristics. For this purpose, a linearized reduced order model including the first three mode shapes (top three traces in Fig. 6) can be obtained from the six-inertia drive-train model [54]. Using modal approximation method, the equivalent model (6), as shown at the bottom of the next page, consisting of three equivalent inertias (J_1, J_2, J_3), two equivalent damping (d_{12}, d_{23}) and two equivalent stiffness (c_{12}, c_{23}) elements is obtained [54]. θ_{12} and θ_{23} represent the relative angle between the two rotating masses. The load torque is $T_L = T_{12} = c_{12}\theta_{12}$ and the wheelset axle torque is $T_{DI} = T_{23} = c_{23}\theta_{23}$, both being referred to the wheelset side. Factors d_D and d_I represent the additional damping on direct and indirect wheels when the adhesion profile changes. According to [51], these damping factors are function of the adhesion force gradient $\frac{\delta\mu}{\delta v_{slip}}$ which is calculated from (7), as shown at the bottom of the next page.

For positive adhesion force gradient, the wheelset adds damping to the drive-train, improving the stability (P_1, P_2, P_3 in Fig. 8a). If the slip velocity is increased beyond the peak of the adhesion coefficient (P'_1, P'_2, P'_3 in Fig. 8a), then the adhesion force gradient becomes negative which reduces the overall damping of the drive-train, increasing the risk of instability. As the damping of the drive-train reduces, the self-resonant frequencies start to appear, their magnitude increasing proportionally to the negative slope of the adhesion coefficient (i.e. $\frac{\delta\mu}{\delta v_{slip}}$).

The eigenvalues state-space wheelset model in (6) can be represented by an equivalent transfer function (8); it consists of a pure integrator while the remaining four poles, as well as the zeros, can be proven to be complex conjugate pairs [51], [54].

$$G_w(s) = \frac{b_4 s^4 + b_2 s^2 + b_0}{s\left(a_4 s^4 + a_2 s^2 + a_0\right)} \tag{8}$$

Coefficients of the transfer function $b_0 \ldots b_4$, $a_0 \ldots a_4$, can be expressed a function of drive-train parameters, the resulting expressions are omitted due to the room constraints [51]. The detailed block diagram of the closed-loop traction drive of the slip velocity control is shown in Fig. 7. The closed-loop block diagram includes the slip velocity control, the torque control, the inverter time delay, the motor electrical and mechanical dynamics respectively which are given by (9)-(12).

$$G_s(s) = k_{ps} + \frac{k_{is}}{s} \tag{9}$$

$$G_c(s) = k_{pi} + \frac{k_{ii}}{s} \tag{10}$$

$$G_e(s) = \frac{1}{\hat{L}_{\sigma s} s + \hat{R}'_s} \tag{11}$$

$$G_m(s) = \frac{1}{\hat{J}_m s + \hat{\beta}} \tag{12}$$

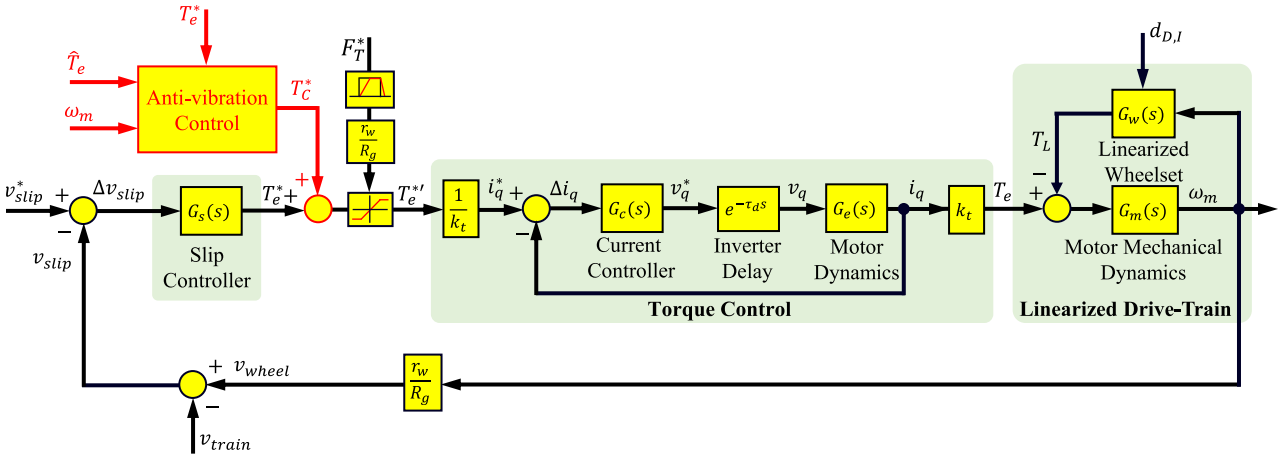

FIGURE 7. Block diagram of slip velocity control coupled with anti-vibration strategy.

where k_{ps} and k_{is} are the proportional and integral (PI) gains for the slip velocity control, respectively; k_{pi} and k_{ii} are the current controller PI gains, respectively; $\hat{L}_{\sigma s}$ and $\hat{R}'_s$ are the estimated stator leakage inductance and resistance, respectively; $\hat{J}_m$ and $\hat{\beta}$ are the estimated motor inertia and friction coefficient, respectively.

To investigate the influence of the wheel-rail contact on the traction drive system, a range of variation of adhesion force gradient -0.12 s/m $< \frac{\delta\mu}{\delta v_{slip}} < 0.12$ s/m is typically used [51]. Closed-loop poles migration of the drive-train for the two extreme cases of -0.12 s/m and 0.12 s/m are shown in Fig. 8b. It is observed that by a proper selection of controller gains, the slip controller is able to damp the first vibration mode (chatter), i.e. associated closed-loop poles are moved to the left-half plane. On the other hand, the second vibration mode (torsional) is insufficiently damped; consequently, drive-train resonance due to this mode will result in torsional vibrations. An additional anti-vibration control for this specific mode is required which will be addressed next.

B. OVERVIEW OF ANTI-VIBRATION METHODS

Anti-vibration control is required to mitigate or suppress this specific torsional vibration mode. The conventional solution is to estimate the dynamic torque on the wheelset axle. A regular PI controller is used to limit the envelope of the oscillation (see Fig. 9a). A limit of 100 kNm is used, this value being obtained at the design stage of the powertrain. PI controller output T_c^* is added to the output of the slip controller (T_e^*, see Fig. 7). In traction mode, the magnitude of the torsional vibration is limited but at the cost of losing traction capability. Also, it is found that the conventional

$$
\begin{aligned}
\dot{X} &= A \cdot X + B \cdot U \\
Y &= C \cdot X + D \cdot U \\
A &= \begin{bmatrix}
\frac{-d_{12}}{J_1} & \frac{d_{12}}{J_1} & 0 & \frac{-c_{12}}{J_1} & 0 \\
\frac{d_{12}}{J_2} & \frac{-(d_{12}+d_{23}+d_D)}{J_2} & \frac{-d_{23}}{J_2} & \frac{c_{12}}{J_2} & \frac{-c_{23}}{J_2} \\
0 & \frac{d_{23}}{J_3} & \frac{-(d_{23}+d_I)}{J_3} & 0 & \frac{-c_{23}}{J_3} \\
1 & -1 & 0 & 0 & 0 \\
0 & 1 & -1 & 0 & 0
\end{bmatrix}; \\
B &= \begin{bmatrix} \frac{R_g}{J_1} & 0 & 0 & 0 & 0 \end{bmatrix}^T; \\
C &= \begin{bmatrix} R_g & 0 & 0 & c_{12} & c_{23} \end{bmatrix}; \quad D = [0] \\
X &= \begin{bmatrix} \omega_1 & \omega_2 & \omega_3 & \theta_{12} & \theta_{23} \end{bmatrix}^T; \\
U &= \begin{bmatrix} T_e & 0 & 0 & 0 & 0 \end{bmatrix}^T; \quad Y = \begin{bmatrix} \omega_m & 0 & 0 & T_{12} & T_{23} \end{bmatrix}^T
\end{aligned} \tag{6}
$$

$$
d_{D,I} = r_w^2 \cdot \frac{m_t \cdot g}{2 \cdot N_m} \cdot \frac{\delta\mu_{D,I}}{\delta v_{slip_{D,I}}} \tag{7}
$$

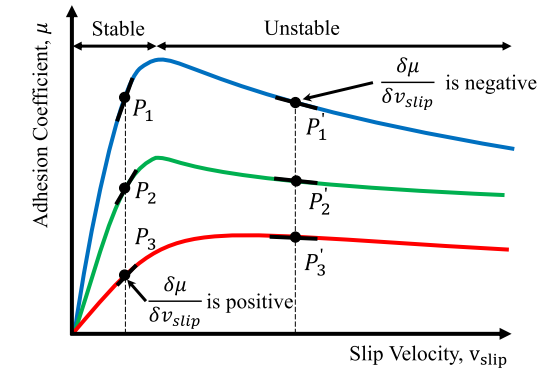

(a) Adhesion coefficient vs. slip speed

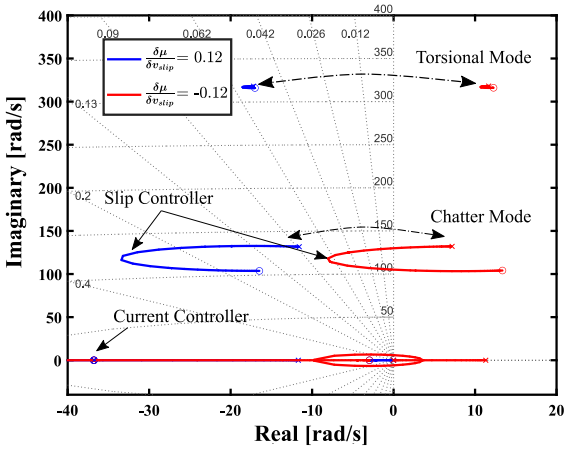

(b) Wheelset pole migration

FIGURE 8. **Influence of wheel-rail contact on the traction drive-train: a) variation of adhesion force gradient over the characteristics curve; b) Root locus plot of the traction drive closed-loop response for the case of the adhesion force gradient being equal −0.12 s/m and 0.12 s/m respectively.**

anti-vibration can effectively damp the vibrations for adhesion curves with negative adhesion gradients bigger than -0.04 s/m (i.e. $\frac{\delta\mu}{\delta v_{slip}} > -0.04$ s/m) [50]. Advanced state-space control approaches based on pole-placement techniques have been recently applied to vibration suppression strategies for negative adhesion gradients less than -0.04 s/m (i.e. $\frac{\delta\mu}{\delta v_{slip}} < -0.04$ s/m). Virtual absorber controller is another promising solution for actively damping not only the torsional vibrations but also improving the whole traction system dynamics [51]. The basic idea of this approach is to emulate a mechanical absorber mounted in the indirect-driven wheel by a feedback controller which is based on the estimated electromagnetic torque ($\hat{T}_e$) and the measured motor speed (ω_m). Combining two or multiple anti-vibration methods (see Fig. 9a) is advantageous to provide high damping to the torsional vibrations even with a very steep adhesion force gradient $\frac{\delta\mu}{\delta v_{slip}} < -0.12$ s/m. However, due to wear, aging, and temperature-dependent of the traction drive-train elements, the vibration frequencies will increase over time. Thus, parameters estimates of the drive-train and the virtual absorber must be very accurate, the equivalent reduced-order model should be automatically adapted accordingly.

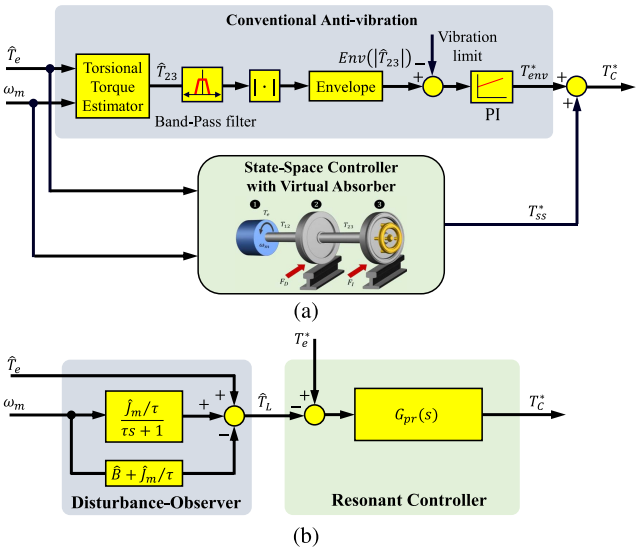

FIGURE 9. **Anti-vibration control strategies based on traction motor variables: a) Existing anti-vibration control; b) Proposed vibration suppression method using PR controller.**

This requires additional natural identification and parameter estimation algorithms which add complexity to the system implementation.

C. PROPOSED PROPORTIONAL-RESONANT ANTI-VIBRATION CONTROL

From the previous discussion, it can be concluded that the traction drive control, without any additional mechanical components, and relying on motor variables only (voltage, current, speed), should be able to suppress the wheelset torsional vibrations. The key aspect of damping the vibrations is to provide the torque correction signal required to adapt the commanded torque according to the wheel-rail operating condition. Since wheel-rail contact act as a disturbance to the motor, a disturbance-observer is used to estimate the motor load torque which contains the vibration transferred from the wheelset side (see fig. 9b). Taking the Laplace transformation for the differential equation of motion on the motor shaft in (13), the load torque is estimated using (14) where τ is the time constant of the low-pass filter in the disturbance observer used for noise reduction in the measured speed. Then, the estimated load torque is subtracted from the commanded torque signal to extract only the vibrating component. Finally, a proportional-resonant (PR) controller is used to suppress the torsional vibrations by injecting the correction torque signal (T_c^*) with the resonance frequency corresponding to the torsional vibration mode.

$$T_L = T_e - \beta\omega_m - J_m\dot{\omega}_m \tag{13}$$

$$\hat{T}_L(s) = \hat{T}_e(s) - \beta\omega_m(s) - J_m s\,\omega_m(s)\left(\frac{1}{\tau s + 1}\right) \tag{14}$$

The use of an ideal resonant controller is not advisable in practice due to its high sensitivity to the frequency of

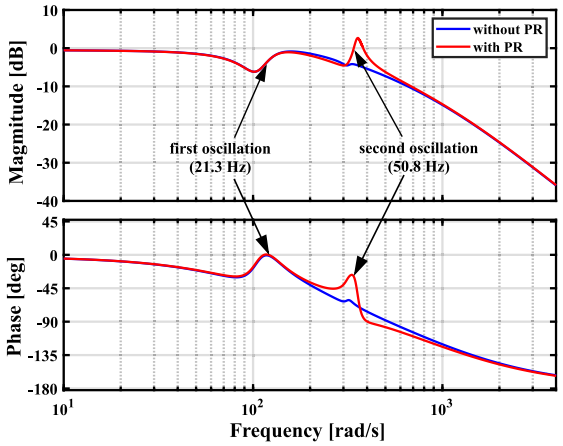

FIGURE 10. Bode plot of $\frac{\omega_m(s)}{\omega_m^*(s)}$ of the slip velocity control without (in blue) and with resonant controller (in red).

the input signal, which might result in instability due to the narrow bandwidths being used. Usually, the resonant controller (PR) given in (15) is preferred, where k_{p_r} and k_{i_r} are the proportional and integral gains, ω_n is the resonant frequency and ω_c is the pass-band frequency range.

$$G_{pr}(s) = k_{p_r} + \frac{2k_{r_r}\omega_c s}{\left(s^2 + 2\omega_c s + \omega_n^2\right)} \tag{15}$$

The effectiveness of the resonant controller can be noticed for the second oscillation (torsional mode) in the bode plot of the closed-loop slip velocity control system (see the red line in Fig. 10). For this specific mode, the PR controller achieves high magnitude attenuation with eliminating the phase delay in the closed-loop response while it does not affect the first oscillation mode. In this way, the torsional (slip-stick) vibrations are suppressed without deteriorating the traction performance and with simple control requirements.

V. SIMULATION RESULTS

To investigate the performance of the proposed vibration suppression method, the entire traction drive system is modeled and simulated using MATLAB/Simulink following the block diagram seen in Fig. 11, with a simulation step of 10 μs. The detailed simulation model consists of the traction drive control, a three-level NPC inverter, the six-inertia wheelset model, the wheel-rail contact characteristics, and the vehicle model. The general specification of the locomotive is given in table 1; the six-mass model parameters are given in table 2 in the appendix A [54]. RFOC and SVPWM with a switching frequency of 1 kHz are used. Current controllers are tuned using the zero/pole cancellation to provide 200 Hz bandwidth, while the slip velocity controller gains are selected from the root locus closed-loop plot in Fig. 8b to achieve better damping of chatter vibration mode. The disturbance-observer filter is chosen to have a time constant of $\tau = 1$ ms while the resonant controller is tuned at $\omega_n = 340$ rad/s with a pass-band width of $\omega_c = 12.5$ rad/s. Selection of gains k_{p_r}, ki_r is therefore extremely

TABLE 1. General specifications of the German class 120 locomotive.

Parameter	Value	Unit
Centenary voltage	15	kV
Centenary frequency	16.7	Hz
Maximum power	4.4	MW
Maximum tractive effort	340	kN
Maximum speed	280	km/h
Weight	84, 000	kg
Gear ratio	4.818	-
Wheel diameter	1.25	m
Number of motors	4	-

challenging due to the variability of operating conditions, a common practice is to follow a trial and error process to achieve sufficient damping to the system for all operating conditions [56].The close-loop controllers gains are given in table 3 in the appendix B.

To initiate the torsional vibrations, the slip velocity command v^*_{slip} is increased from 0.1 to 1 m/s, the adhesion force gradient changing from positive to negative (see Fig. 8a). Fig. 12a shows the system response when it enters the unstable region of the adhesion-slip curve. The torsional vibration appears after ≈ 3 seconds when 1 m/s slip velocity is commanded. In general, the more negative is the gradient, the sooner vibration will start. Fig. 12b shows the frequency spectrum of torque and speed signals when the system is in vibration mode. Vibration frequency is around 50.8 Hz, which matches the results from mode shape analysis in subsection III-C. The highest torque vibration occurs at the wheelset axle ($T_{DI} = 40$ kNm), the magnitude increasing proportionally to the (negative) adhesion force gradient. It can be also noticed the traction motor torque and the measured speed contains the vibration information, which is required to detect and further control the torsional vibration.

The effectiveness of the proposed method in the same scenario is shown in Fig. 13a. PR controller is first enabled and disabled gradually (6 s $\leq t \leq$ 11 s), and latter suddenly at $t = 14$ s, see Fig. 13a-bottom). The activation process is done using a sliding factor (varying from 0 to 1) where it is multiplied by the PR output signal. It is seen that the proposed PR controller damps the torsional vibration, no adverse effects are observed due to sudden activation/deactivation. It is also seen that if adverse adhesion conditions remain, torsional vibrations resume a few seconds after PR control is disabled. Therefore, it is advisable to keep the PR controller enabled all the time.

A potential concern for the proposed method would be the noise in the estimated motor speed. Incremental encoders are widely used in railway. Encoder signals are normally converted into pulses to ease their acquisition and processing. However, since the encoder provides a position signal, some type of differentiation is required to obtain the angular speed. Due to the discrete nature of encoder signal, differentiation will result in quantization noise in the estimated speed [57]. In this work, speed is estimated by combining periodimeter and frequencimeter methods [57], [58].

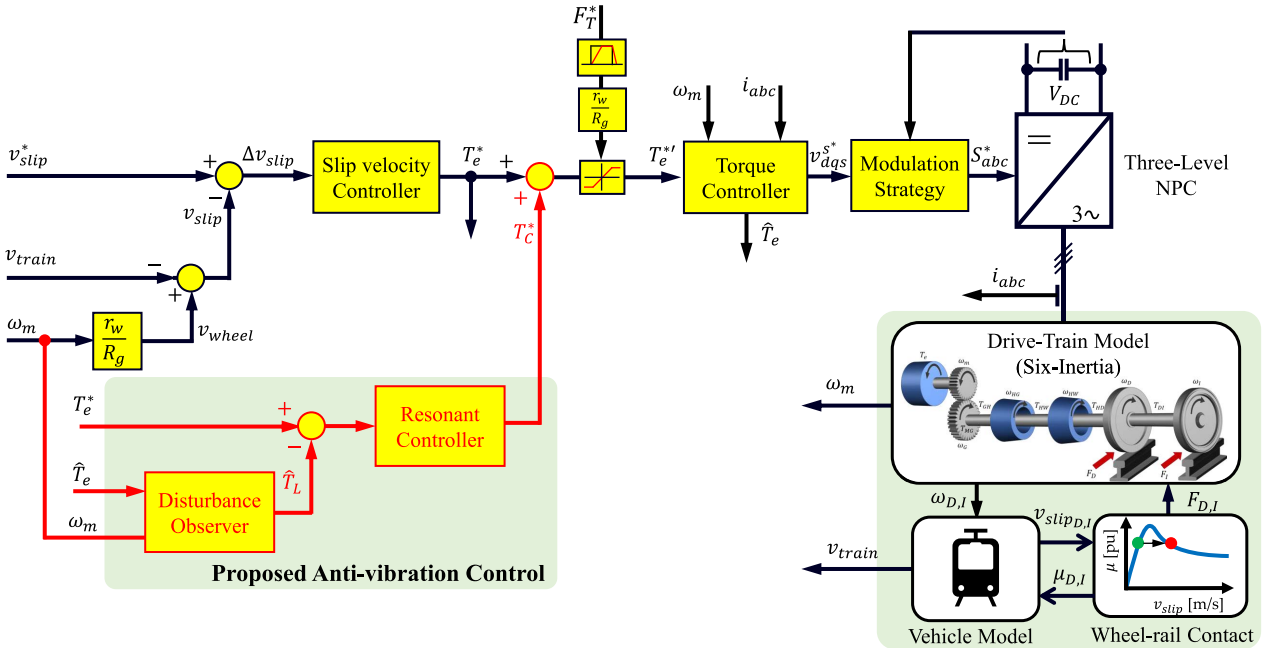

FIGURE 11. Schematic representation of the complete traction drive simulation model with the proposed anti-vibration control.

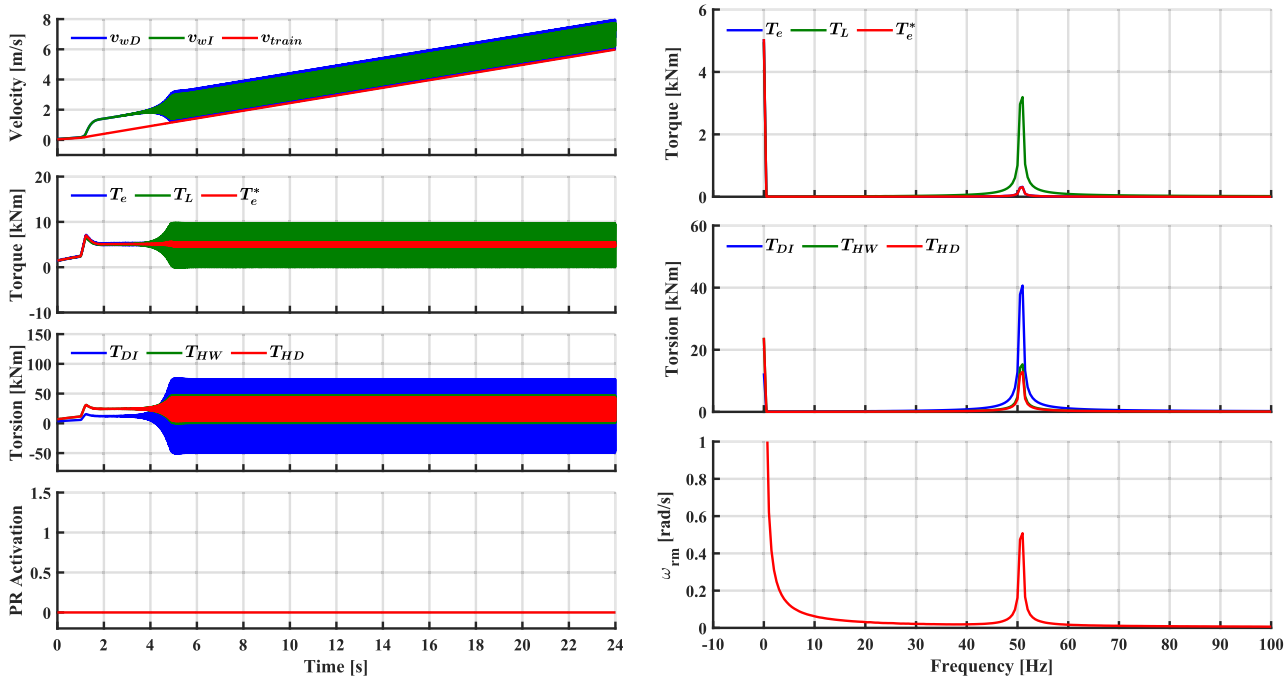

(a) Time response (b) |FFT|

FIGURE 12. Response of the slip velocity control while commanding 1 [m/s] at t = 1 s.

The effect of quantization noise in the estimated speed is shown in Fig. 13. A rotary incremental encoder with 4-channels 256 pulse per revolution (PPR) was used [59]. Comparing the results with ideal speed measurement in Fig. 13a and considering quantization noise in Fig. 13b, it is observed that the main difference occurs when the PR is activated suddenly. On the contrary, almost no difference is observed if PR is activated progressively, or when it remains enabled.

The proposed method is validated against the conventional vibration mitigation method shown in Fig. 9a where the vibration limit is set to 20 kNm (see Fig. 14 vs. Fig. 13a from $t = 6 \rightarrow 11$ s and $t = 14 \rightarrow 24$ s). A clear observation is the loss of traction torque in the conventional suppression

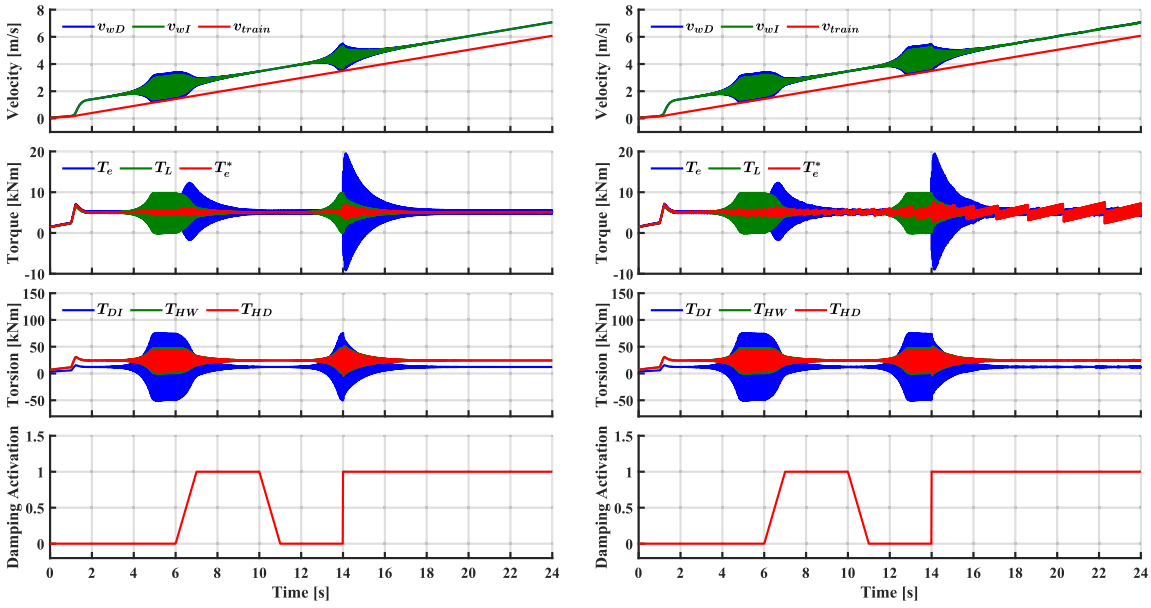

FIGURE 13. Response of the proposed method when PR is activated/deactivated gradually ($t = 6$ s $\rightarrow$ $t = 10$ s), and suddenly ($t = 14$). (a) With ideal speed measurement; (b) using and incremental encoder for speed measurement.

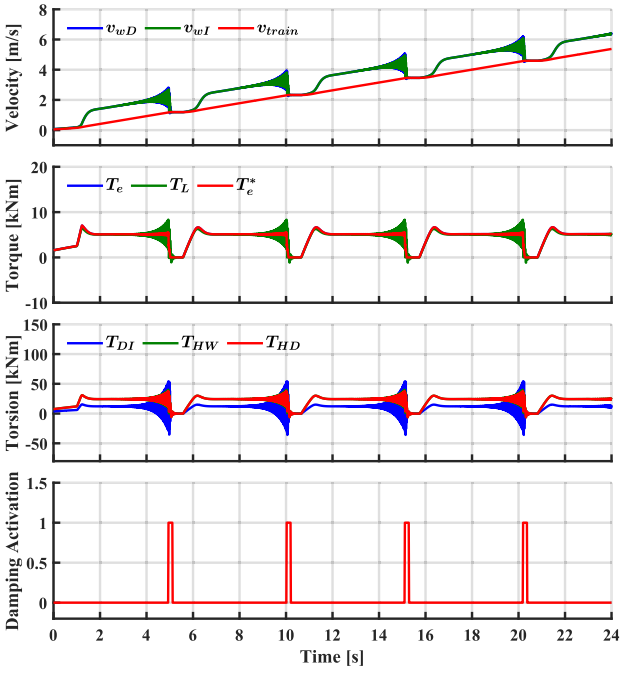

FIGURE 14. Response of conventional torsional vibration mitigation method.

method (see Fig. 14) to damp the oscillation. However, after suppressing the oscillation and restoring the traction torque capability, the oscillations appear continuously as the slip velocity command remains at the same operating point with the negative slope of the adhesion curve (i.e. 1 m/s). In the contrast, the proposed suppression method maximized the utilisation of the traction torque with completely suppressing the oscillations as seen in Fig. 13a.

Evaluation of the proposed method under varying conditions will be discussed in the following subsections:

A. EFFECTS OF VARYING SLIP VELOCITY AND WHEEL-RAIL CONDITION

Variations in the slip command can occur when the locomotive has an outer control loop implementing maximum traction force searching. This might drive the operating point into the unstable region where the torsional vibration arises. An example of the response of the proposed method to changes in the slip velocity is shown in Fig. 15a. Wheel-rail contact is modeled as profile 1 in the adhesion curve shown in Fig. 8a. The traction torque is increased from 5 kNm to 5.8 kNm by decreasing the slip velocity to 0.5 m/s. Then, the torque is decreased to 4.6 kNm when operating at the slip of 1.5 m/s. The maximum adhesion force can be achieved when $v_{slip} = 0.25$ m/s with this specific adhesion profile. However, the resonant controller was able to dampen the wheelset oscillations for all commanded slip velocities.

Variations of wheel-rail contact conditions have been reported as the main mechanism for exciting the wheelset natural frequencies leading to dynamic torque oscillations [31], [60]. Fig. 15b shows the response when the contact condition changes between dry to wet (profiles 1 to 3 in Fig. 8a). The change can occur for one wheel or both wheels, this second case is shown in the figure. The change from dry to wet decreases the adhesion force gradient $\frac{\delta\mu}{\delta v_{slip}}$ of both wheels initiating oscillations in the counter phase. It is observed from Fig. 15b that the torsional control reacts reducing torque from 5 kNm to 1 kNm at $t = 8$ s. This will keep the slip velocity at 1 m/s avoiding excessive slip. Once the wheel-rail contact returns to a dry condition, the

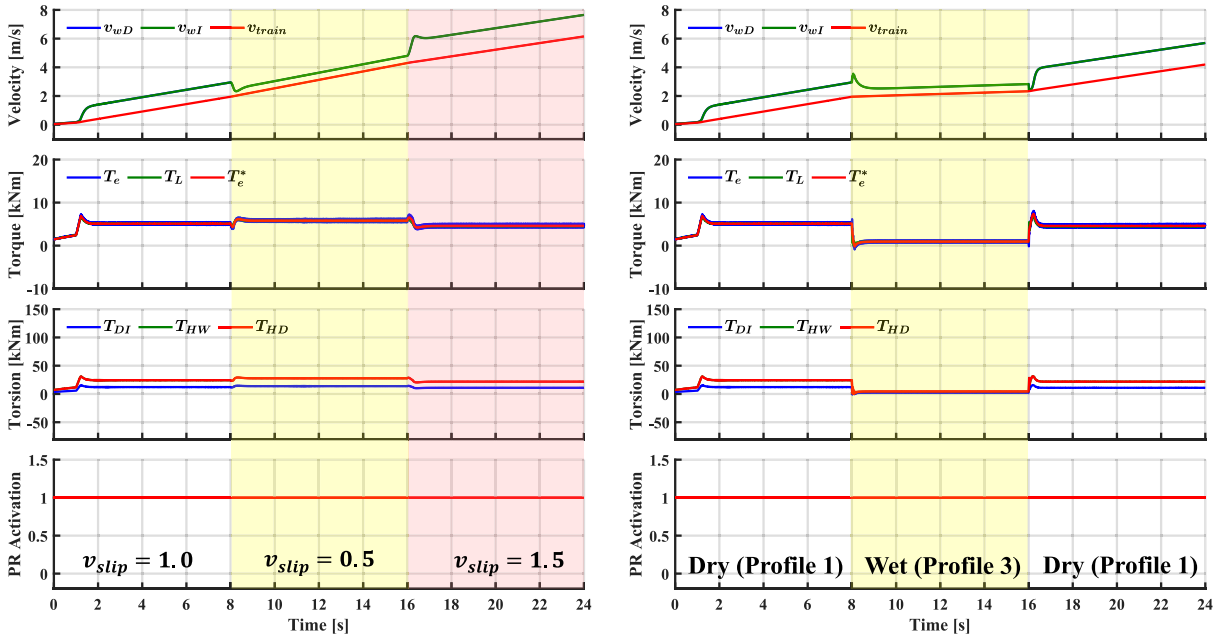

(a) Slip velocity changes (b) Adhesion profile changes

FIGURE 15. Response of the proposed method at different operating conditions.

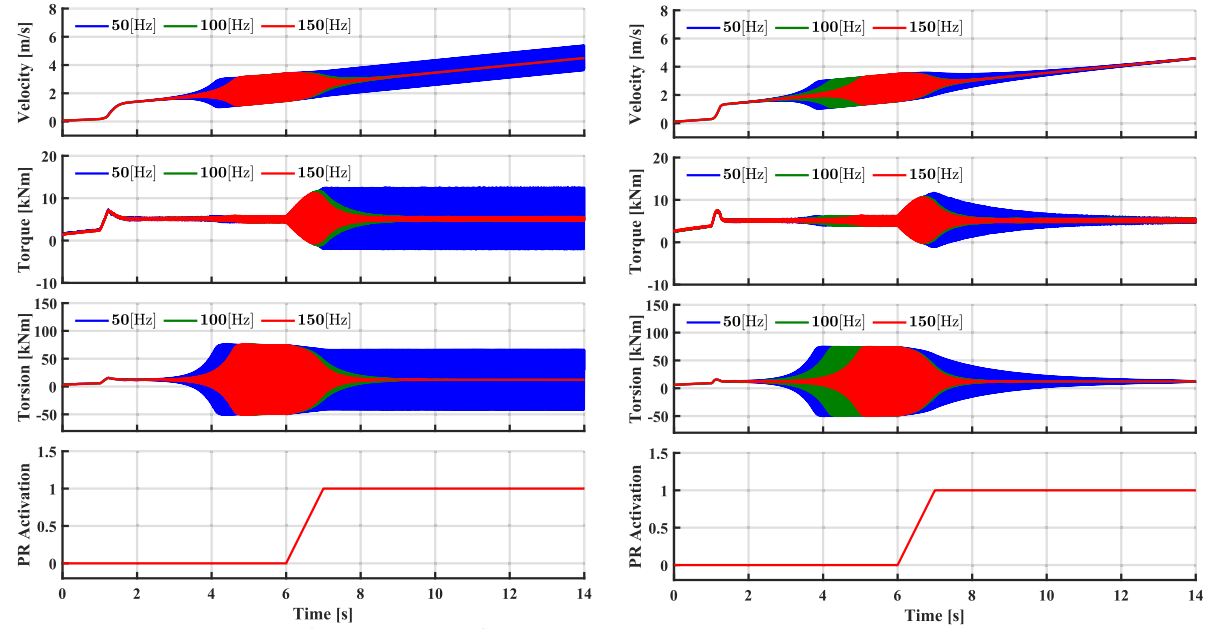

(a) $k_{p_{s1}} = 4.7 \times 10^3, k_{i_{s1}} = 1.4 \times 10^4$ (b) $k_{p_{s2}} = 2k_{p_{s1}}, k_{i_{s2}} = 2k_{i_{s1}}$

FIGURE 16. Response of the proposed method with changing the current controller bandwidth (150, 100 and 50 Hz) for two different tuning sets of the slip velocity controller.

motor torque returns to its initial value. Again, the proposed method is seen to provide a good response under challenging operating conditions.

B. EFFECT OF THE DRIVE CONTROL BANDWIDTH

In the previous simulations, fast torque control is assumed, which is achieved thanks to the use of vector control with 200 Hz bandwidth for current regulators. Frequently, drive control is switched to scalar methods at high speed, especially when the inverter is operated in the overmodulation region close to the voltage limit. A drawback of scalar control is the slow dynamic response of the torque control loop.

Fig. 16b shows the effect of the torque control bandwidth, with the same slip control setup shown in Fig. 11. It is clear that the lower the bandwidth, the longer the time needed to fully suppress the vibration. Interestingly, it is found that for torque control bandwidths below $<\approx$ 60 Hz, oscillations are not properly cancelled. By doubling the slip controller

gains, the control system is able to damp the oscillation for all bandwidths (50 to 150 Hz) (see Fig. 16a). However, increasing the slip velocity controller gains is not desired as it will amplify the feedback noise coming from the motor speed measurement and might also lead to oscillations in practice.

A potential concern when high bandwidth current regulators are used, is the presence of electrical noise in the measured currents. The reduce this risk, oversampling of current sensors was used [61]. A field-programmable gate array (FPGA) measures the signal every 5 μs, and averages the measurement over the whole control period. The PWM operates with a period of 1 ms and with double update, 100 samples being therefore averaged each control period. This will reduce the noise in the signals to negligible levels [62], [63].

VI. CONCLUSION

Design and analysis of dynamic torque control for railways have been addressed in this paper. Modeling of the electric drive, mechanical drive-train, and vehicle considering slippage and vibrations phenomena have been presented. The conclusions of the analysis can be summarized as follows:

- The adhesion force gradient is the key factor for torsional vibration phenomena. This factor is often unpredictable. Moving this factor from positive to negative values pushes the system to the stability limit or even towards the instability.
- Operating with negative adhesion force gradient will excite the resonance frequencies of the mechanical elements in the drive-train, their severity increasing proportionally to the negative slope of the adhesion curve.
- The first two resonance frequencies are the most affecting modes on the motor shaft and the press-fit of the wheelset axle. These two modes should be eliminated or kept as minimum value as possible to avoid fatigue and failure of the drive-train element.
- Equipping the electric drive with a slip controller, besides preventing the wheel from slipping on the rail, can perfectly dampen the first resonance mode (chatter mode) and return the system to the stable region. However, the slip control has less influence on the second resonance mode occurring between the two wheels (torsional mode).
- Reducing the motor torque is one of the simplest solutions to damp the torsional resonance mode but at the cost of losing traction force. Therefore, advanced control techniques are required to be added in parallel with the slip controller.

An anti-vibration method using a resonant controller has been proposed in this paper. A PR controller is used for this purpose, whose output is added to the torque command used to provide traction effort. Torque oscillations are obtained from the estimated traction motor load torque. Only the estimated electromagnetic torque and the measured motor speed are required, no additional sensors/cabling or drive-train state observers are therefore needed. The proposed anti-vibration control is robust against variations of slip velocity and under changing wheel-rail conditions providing maximum available traction with no interruption. It has also been shown that proper operation of the proposed method requires torque control bandwidths in the range of 60 Hz or higher. As a general conclusion, higher bandwidths in the slip controller will improve the overall performance of the traction control system using the proposed method.

APPENDIX A
MECHANICAL DRIVE-TRAIN PARAMETERS

TABLE 2. Six-inertia drive-train model parameters of the German class 120 locomotive referred to the wheelset side [54], [55].

Moment of inertia	**Symbol**	**Value**	**Unit**
Traction motor	j_M	466.6	Kgm^2
Gear	j_G	55	Kgm^2
Half of hollow shaft to the gearbox side	j_{HG}	10.13	Kgm^2
Half of hollow shaft to the wheel side	j_{HW}	9.72	Kgm^2
Direct wheel and coupling	j_D	163	Kgm^2
Indirect wheel	j_I	157.3	Kgm^2
Torsional stiffness	**Symbol**	**Value**	**Unit**
Motor shaft	c_{MG}	88.12×10^6	Nm
Coupling (Gear side)	c_{GH}	15.1×10^6	Nm
Hollow shaft	c_{HW}	10.1×10^6	Nm
Coupling (Wheel side)	c_{HD}	15.7×10^6	Nm
Wheelset axle	c_{DI}	7.06×10^6	Nm
Torsional damping ratio	**Symbol**	**Value**	**Unit**
Motor shaft	d_{MG}	920.3×10^6	Nms
Coupling (Gear side)	d_{GH}	4730.8×10^6	Nms
Hollow shaft	d_{HW}	105.5×10^6	Nms
Coupling (Wheel side)	d_{HD}	11731.4×10^6	Nms
Wheelset axle	d_{DI}	73.7×10^6	Nms

APPENDIX B
CONTROLLERS GAINS

TABLE 3. Closed-loop control gains of the simulated model.

Regulator type	**Controller gain**	**Value**
Current	k_{p_i}	2.2281
	k_{i_i}	81.9413
Slip velocity	k_{p_s}	4.7×10^3
	k_{i_s}	1.4×4
Anti-vibration	k_{p_r}	0.1
	k_{r_r}	2

REFERENCES

[1] European Union Agency for Railways. (2018). *Report on Railway Safety and Interoperability in the EU*. [Online]. Available: https://www.era.europa.eu/sites/default/files/library/docs/safety_inter%operability_progress_reports/railway_safety_and_interoperability_in_eu_2018_en%.pdf

[2] J. Zeng and P. Wu, "Study on the wheel/rail interaction and derailment safety," *Wear*, vol. 265, nos. 9–10, pp. 1452–1459, 2008.

[3] J. Santamaria, E. Vadillo, and J. Gomez, "Influence of creep forces on the risk of derailment of railway vehicles," *Vehicle Syst. Dyn.*, vol. 47, no. 6, pp. 721–752, 2009.

[4] K. Kondo, "Anti-slip control technologies for the railway vehicle traction," in *Proc. IEEE Vehicle Power Propuls. Conf.*, Oct. 2012, pp. 1306–1311.

[5] P. Pichlík and J. Zdeněk, "Overview of slip control methods used in locomotives," *Trans. Electr. Eng.*, vol. 3, no. 2, pp. 38–43, 2014.

[6] U. Caglar, G. Metin, and B. Seta, "Comparison of the re-adhesion control strategies in high-speed train," *Proc. Inst. Mech. Eng., I, J. Syst. Control Eng.*, vol. 232, no. 1, pp. 92–105, 2018.

[7] O. Polach, "Creep forces in simulations of traction vehicles running on adhesion limit," *Wear*, vol. 258, nos. 7–8, pp. 992–1000, 2005.

[8] D.-Y. Park, M.-S. Kim, D.-H. Hwang, J.-H. Lee, and Y.-J. Kim, "Hybrid re-adhesion control method for traction system of high-speed railway," in *Proc. 5th Int. Conf. Electr. Mach. Syst. (ICEMS)*, vol. 2, Aug. 2001, pp. 739–742.
[9] T. WATANABE, "Anti-slip readhesion control with presumed adhesion force-method of presuming adhesion force and running test results of high-speed shinkansen train," *Quart. Rep. RTRI*, vol. 41, no. 1, pp. 32–36, 2000.
[10] J. Huang, J. Xiao, and H. Weiss, "Simulation study on adhesion control of electric locomotives based on multidisciplinary virtual prototyping," in *Proc. IEEE Int. Conf. Ind. Technol.*, Apr. 2008, pp. 1–4.
[11] M. Yamashita and T. Soeda, "Anti-slip re-adhesion control method for increasing the tractive force of locomotives through the early detection of wheel slip convergence," in *Proc. 17th Eur. Conf. Power Electron. Appl. (EPE ECCE-Eur.)*, Sep. 2015, pp. 1–10.
[12] A. D. Cheok and S. Shiomi, "A fuzzy logic based anti-skid control system for railway applications," in *Proc. 2nd Int. Conf. Knowl.-Based Intell. Electron. Syst. Proc. (KES)*, vol. 1, Apr. 1998, pp. 195–201.
[13] A. D. Cheok and S. Shiomi, "Combined heuristic knowledge and limited measurement based fuzzy logic antiskid control for railway applications," *IEEE Trans. Syst., Man, Cybern. C, Appl. Rev.*, vol. 30, no. 4, pp. 557–568, Nov. 2000.
[14] T. Watanabe and M. Yamashita, "A novel anti-slip control without speed sensor for electric railway vehicles," in *Proc. 27th Annu. Conf. IEEE Ind. Electron. Soc. (IECON)*, vol. 2, Dec. 2001, pp. 1382–1387.
[15] K. Ohishi, Y. Ogawa, I. Miyashita, and S. Yasukawa, "Anti-slip re-adhesion control of electric motor coach based on force control using disturbance observer," in *Proc. Conf. Rec. IEEE Ind. Appl. Conf.*, vol. 2, Oct. 2000, pp. 1001–1007.
[16] M. Spiryagin, K. S. Lee, and H. H. Yoo, "Control system for maximum use of adhesive forces of a railway vehicle in a tractive mode," *Mech. Syst. signal Process.*, vol. 22, no. 3, pp. 709–720, 2008.
[17] K. Ohishi, T. Hata, T. Sano, and S. Yasukawa, "Realization of anti-slip/skid re-adhesion control for electric commuter train based on disturbance observer," *IEEJ Trans. Electr. Electron. Eng.*, vol. 4, no. 2, pp. 199–209, 2009.
[18] L. Diao, L. Zhao, Z. Jin, L. Wang, and S. M. Sharkh, "Taking traction control to task: High-adhesion-point tracking based on a disturbance observer in railway vehicles," *IEEE Ind. Electron. Mag.*, vol. 11, no. 1, pp. 51–62, Mar. 2017.
[19] P. Pichlik and J. Zdenek, "Locomotive wheel slip control method based on an unscented Kalman filter," *IEEE Trans. Veh. Technol.*, vol. 67, no. 7, pp. 5730–5739, Jul. 2018.
[20] P. Pichlik and J. Bauer, "Adhesion characteristic slope estimation for wheel slip control purpose based on UKF," *IEEE Trans. Veh. Technol.*, vol. 70, no. 5, pp. 4303–4311, 2021.
[21] M. Buscher, *Radschlupfregelung Zur Maximalen Kraftschlussausnutzung Bei Elektrischen Traktionsantrieben*. Aachen, Germany: Verlag Shaker, 1995.
[22] H. Ryoo, S. Kim, G. Rim, Y. Kim, and M. Kim, "Novel anti-slip/slide control algorithm for Korean high-speed train," in *Proc. 29th Annu. Conf. IEEE Ind. Electron. Soc. (IECON)*, vol. 3, Nov. 2003, pp. 2570–2574.
[23] X. Fang, S. Lin, Z. Yang, F. Lin, H. Sun, and L. Hu, "Adhesion control strategy based on the wheel-rail adhesion state observation for high-speed trains," *Electronics*, vol. 7, no. 5, p. 70, 2018.
[24] S. Sadr, D. A. Khaburi, and J. Rodríguez, "Predictive slip control for electrical trains," *IEEE Trans. Ind. Electron.*, vol. 63, no. 6, pp. 3446–3457, Jun. 2016.
[25] K. Can, H. Jingchun, D. Wenqi, and W. Xiaokang, "Adhesion control method based on optimal slip velocity searching and tracking," in *Proc. 14th IEEE Int. Conf. Electron. Meas. Instrum. (ICEMI)*, Nov. 2019, pp. 1200–1207.
[26] S. H. Park, J. S. Kim, J. J. Choi, and H. Yamazaki, "Modeling and control of adhesion force in railway rolling stocks," *IEEE Control Syst. Mag.*, vol. 28, no. 5, pp. 44–58, Oct. 2008.
[27] T. Ishrat, G. Ledwich, M. Vilathgamuwa, and P. Borghesani, "Identification scheme of maximum traction force using recursive least square for traction control in electric locomotives," in *Proc. IEEE 12th Int. Conf. Power Electron. Drive Syst. (PEDS)*, Dec. 2017, pp. 1–120.
[28] Z. Huang, W. Du, B. Chen, K. Gao, Y. Liu, X. Tang, and Y. Yang, "An online super-twisting sliding mode anti-slip control strategy," *Energies*, vol. 13, no. 7, p. 1823, 2020.
[29] X. Wen, J. Huang, and S. Zhang, "Anti-slip re-adhesion control strategy of electric locomotive based on distributed MPC," in *Proc. IEEE 21st Int. Conf. High Perform. Comput. Commun. IEEE 17th Int. Conf. Smart City, IEEE 5th Int. Conf. Data Sci. Syst. (HPCC/SmartCity/DSS)*, Aug. 2019, pp. 2708–2713.
[30] A. Zirek and A. Onat, "A novel anti-slip control approach for railway vehicles with traction based on adhesion estimation with swarm intelligence," *Railway Eng. Sci.*, vol. 28, no. 4, pp. 346–364, 2020.
[31] T. Fridrichovskỳ and B. Šulc, "Investigation of torsional oscillations in railway vehicles," in *Proc. MATEC Web Conf.*, vol. 76, 2016, Art. no. 02052.
[32] H. Wu, P. Wu, K. Xu, J. Li, and F. Li, "Research on vibration characteristics and stress analysis of gearbox housing in high-speed trains," *IEEE Access*, vol. 7, pp. 102508–102518, 2019.
[33] M. Bruha and Z. Peroutka, "Torsional vibration in large variable speed drive systems: Origin and mitigation methods," in *Proc. 17th Eur. Conf. Power Electron. Appl. (EPE ECCE-Eur.)*, Sep. 2015, pp. 1–10.
[34] J. Pacas, A. John, and T. Eutebach, "Automatic identification and damping of torsional vibrations in high-dynamic-drives," in *Proc. IEEE Int. Symp. Ind. Electron. (ISIE)*, vol. 1, Dec. 2000, pp. 201–206.
[35] S. N. Vukosavic and M. R. Stojic, "Suppression of torsional oscillations in a high-performance speed servo drive," *IEEE Trans. Ind. Electron.*, vol. 45, no. 1, pp. 108–117, Feb. 1998.
[36] K.-K. Shyu and C.-Y. Chang, "Modified FIR filter with phase compensation technique to feedforward active noise controller design," *IEEE Trans. Ind. Electron.*, vol. 47, no. 2, pp. 444–453, Apr. 2000.
[37] L. Litwin, "FIR and IIR digital filters," *IEEE Potentials*, vol. 19, no. 4, pp. 28–31, Oct. 2000.
[38] T. Ohmae, T. Matsuda, M. Kanno, K. Saito, and T. Sukegawa, "A microprocessor-based motor speed regulator using fast-response state observer for reduction of torsional vibration," *IEEE Trans. Ind. Appl.*, vol. IA-23, no. 5, pp. 863–871, Sep. 1987.
[39] Y. Hori, H. Iseki, and K. Sugiura, "Basic consideration of vibration suppression and disturbance rejection control of multi-inertia system using SFLAC (state feedback and load acceleration control)," *IEEE Trans. Ind. Appl.*, vol. 30, no. 4, pp. 889–896, Jul./Aug. 1994.
[40] K. Sugiura and Y. Hori, "Vibration suppression in 2-and 3-mass system based on the feedback of imperfect derivative of the estimated torsional torque," *IEEE Trans. Ind. Electron.*, vol. 43, no. 1, pp. 56–64, Feb. 1996.
[41] M. Neshati, T. Jersch, and J. Wenske, "Model based active damping of drive train torsional oscillations for a full-scale wind turbine nacelle test rig," in *Proc. Amer. Control Conf. (ACC)*, Jul. 2016, pp. 2283–2288.
[42] J.-K. Ji and S.-K. Sul, "Kalman filter and LQ based speed controller for torsional vibration suppression in a 2-mass motor drive system," *IEEE Trans. Ind. Electron.*, vol. 42, no. 6, pp. 564–571, Dec. 1995.
[43] E. Omine, T. Goya, U. Akie, T. Senjyu, A. Yona, N. Urasaki, and T. Funabashi, "Torsional torque suppression of decentralized generators using h∞ observer," *Renew. Energy*, vol. 35, no. 9, pp. 1908–1913, 2010.
[44] Y. Wang, Q. Zheng, H. Zhang, and M. Chen, "The LQG/LTR control method for turboshaft engine with variable rotor speed based on torsional vibration suppression," *J. Low Freq. Noise, Vibrat. Act. Control*, vol. 39, no. 4, pp. 1145–1158, 2020.
[45] T. Hirotsu, S. KASAI, and H. TAKAI, "Self-excited vibration during slippage of parallel cardan drives for electric railcars: Vibration, control engineering, engineering for industry," *JSME Int. J.*, vol. 30, no. 266, pp. 1304–1310, 1987.
[46] M. Lata, "The modern wheelset drive system and possibilities of modelling the torsion dynamics," *Transport*, vol. 23, no. 2, pp. 172–181, 2008.
[47] R. Konowrocki and T. Szolc, "An analysis of the self-excited torsional vibrations of the electromechanical drive system," *Vib. Phys. Syst.*, vol. 27, pp. 187–194, 2016.
[48] K. Xu, J. Zeng, and L. Wei, "An analysis of the self-excited torsional vibration of high-speed train drive system," *J. Mech. Sci. Technol.*, vol. 33, no. 3, pp. 1149–1158, 2019.
[49] T. Mei, J. Yu, and D. Wilson, "A mechatronic approach for anti-slip control in railway traction," *IFAC Proc. Volumes*, vol. 41, no. 2, pp. 8275–8280, 2008.
[50] M. Fleischer and K. Kondo, "Slip-stick vibration suppression by modal state control for traction drive-trains," *IEEJ J. Ind. Appl.*, vol. 5, no. 1, pp. 1–9, 2016.
[51] M. Fleischer, R. W. De Doncker, and D. Abel, "Traction control for railway vehicles," Institut für Stromrichtertechnik und Elektrische Antriebe, Aachen Univ., Aachen, Germany, 2019, vol. 128.
[52] R. Teichmann and S. Bernet, "A comparison of three-level converters versus two-level converters for low-voltage drives, traction, and utility applications," *IEEE Trans. Ind. Appl.*, vol. 41, no. 3, pp. 855–865, May 2005.
[53] A. F. Abouzeid, J. M. Guerrero, A. Endemano, I. Muniategui, D. Ortega, I. Larrazabal, and F. Briz, "Control strategies for induction motors in railway traction applications," *Energies*, vol. 13, no. 3, p. 700, 2020.

[54] H. J. Schwartz, *Regelung Der Radsatzdrehzahl Zur Maximalen Kraftschlussausnutzung Bei Elektrischen Triebfahrzeugen*. Düsseldorf, Germany: VDI-Verlag, 1992.
[55] F. Trimpe, S. Lück, R. Naumann, and C. Salander, "Simulation of torsional vibration of driven railway wheelsets respecting the drive control response on the vibration excitation in the wheel-rail contact point," *Vibration*, vol. 4, no. 1, pp. 30–48, 2021. [Online]. Available: https://www.mdpi.com/2571-631X/4/1/3
[56] R. Chattopadhyay, A. De, and S. Bhattacharya, "Comparison of PR controller and damped pr controller for grid current control of LCL filter based grid-tied inverter under frequency variation and grid distortion," in *Proc. IEEE Energy Convers. Congr. Expo. (ECCE)*, Sep. 2014, pp. 3634–3641.
[57] F. Briz, J. Cancelas, and A. Diez, "Speed measurement using rotary encoders for high performance ac drives," in *Proc. 20th Annu. Conf. IEEE Ind. Electron. (IECON)*, vol. 1, Sep. 1994, pp. 538–542.
[58] Y. Li, F. Gu, G. Harris, A. Ball, N. Bennett, and K. Travis, "The measurement of instantaneous angular speed," *Mech. Syst. Signal Process.*, vol. 19, no. 4, pp. 786–805, 2005.
[59] *Lenord + Bauer.Speed Sensors & Rotary Pulse Encoders: Rail Speed Sensor Gel 2477*. Accessed: Feb. 14, 2022. [Online]. Available: https://www.sensorprod.com/lenord/speed-sensor-gel-2477.php
[60] F. Trimpe and C. Salander, "Wheel-rail adhesion during torsional vibration of driven railway wheelsets," *Vehicle Syst. Dyn.*, vol. 59, no. 5, pp. 785–799, 2021.
[61] J. Böcker and O. Buchholz, "Can oversampling improve the dynamics of PWM controls?" in *Proc. IEEE Int. Conf. Ind. Technol. (ICIT)*, Feb. 2013, pp. 1818–1824.
[62] M.-W. Naouar, E. Monmasson, A. A. Naassani, I. Slama-Belkhodja, and N. Patin, "FPGA-based current controllers for ac machine drives—A review," *IEEE Trans. Ind. Electron.*, vol. 54, no. 4, pp. 1907–1925, Jul. 2007.
[63] E. Monmasson, L. Idkhajine, and M. W. Naouar, "FPGA-based controllers," *IEEE Ind. Electron. Mag.*, vol. 5, no. 1, pp. 14–26, Mar. 2011.

AHMED FATHY ABOUZEID (Member, IEEE) received the B.S. and M.S. degrees in electrical engineering from Port Said University, Port Said, Egypt, in 2012 and 2017, respectively. He is currently pursuing the Ph.D. degree with the Department of Electrical, Electronic and Computer Engineering, University of Oviedo, Gijón, Spain. In 2013, he joined the Department of Electrical Engineering, Port Said University, as a Teaching Assistant. He is on leave with the Department of Electrical Engineering as an Assistant Lecturer. He is partially supported by the Scholarship from the Ministry of Higher Education and Scientific Research of Egypt. His research interests include power converters and ac drives, electric traction, and renewable energy systems.

JUAN M. GUERRERO (Senior Member, IEEE) received the M.E. degree in industrial engineering and the Ph.D. degree in electrical and electronic engineering from the University of Oviedo, Gijón, Spain, in 1998 and 2003, respectively. Since 1999, he has been occupied different teaching and research positions with the Department of Electrical, Computer and Systems Engineering, University of Oviedo, where he is currently an Associate Professor. From February 2002 to October 2002, he was a Visiting Scholar at the University of Wisconsin, Madison. From June 2007 to December 2007, he was a Visiting Professor at Tennessee Technological University, Cookeville. His research interests include control of electric drives and power converters, electric traction, and renewable energy generation. He is an Associate Editor of the IEEE TRANSACTIONS ON INDUSTRY APPLICATIONS.

IBAN VICENTE-MAKAZAGA graduated in electrical engineering from the University of Mondragon, Mondragon, Spain, in 2003, and the M.S. and Ph.D. degrees from The University of Manchester, U.K., in 2004 and 2009, respectively. He joined Ingeteam Power Technology (formerly TEAM), Zamudio, Spain, where he currently works as a Control and Regulation Engineer involved in railway traction control for trams, locomotives, and EMU-s. His current research interests include power converter and advanced control drives, modulation techniques, machine parameters, speed estimation techniques, and railway research issues, such as AC catenary stability and mechanical vibrations in the drive-train.

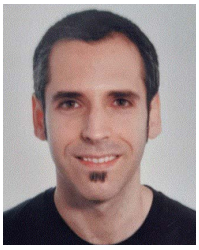

IKER MUNIATEGUI-ASPIAZU received the Industrial Technical Engineering degree (electronic design specialty) and the Industrial Automatics and Electronics Engineering degree from the University of Mondragon, Mondragon, Spain, in 2004 and 2007, respectively. In September 2006, he joined Ingeteam Power Technology (formerly TEAM), Zamudio, Spain, where he worked as a Control and Regulation Engineer and he is currently a Control and Regulation Manager of the Traction Department. His current research interests include power converter and advanced control drives, modulation techniques, and railway research issues, such as AC catenary stability and mechanical vibrations in the drive-train.

AITOR ENDEMAÑO-ISASI received the Industrial Technical Engineering degree (electronic design specialty) and the Industrial Automatics and Electronics Engineering degree from the University of Mondragon, Mondragon, Spain, in 1997 and 2000, respectively, and the Ph.D. degree from Heriot-Watt University, Edinburgh, U.K., in 2003. In 2003, he joined the Traction Department, Ingeteam Power Technology (formerly TEAM), Zamudio, Spain, where he has been a Control and Regulation Engineer (since then), involved in several traction control design projects for trams, locomotives, and EMU-s. His current research interests include power converter and advanced control drives, modulation techniques, and railway research issues, such as AC catenary stability and mechanical vibrations in the drive-train.

FERNANDO BRIZ (Senior Member, IEEE) received the M.S. and Ph.D. degrees from the University of Oviedo, Gijón, Spain, in 1990 and 1996, respectively. He is currently a Full Professor with the Department of Electrical, Computer and Systems Engineering, University of Oviedo. His research interests include electronic power converters and ac drives, power systems, machine monitoring and diagnostics, and digital signal processing. He is a member of the Executive Board of ECCE. He was a recipient of the IEEE TRANSACTIONS ON INDUSTRY APPLICATIONS Award and the nine IEEE Industry Applications Society Conference and IEEE Energy Conversion Congress and Exposition Prize Paper Awards. He is the Chair of the Industrial Power Conversion System Department (IPCSD) of the IAS. He is the Past Chair of the Industrial Drives Committee of IPCSD. He has served for scientific committees and as the Vice Chair or the Technical Program Chair for several conferences, including ECCE, IEMDC, ICEM, ICEMS, and SLED. He is the Deputy Editor-in-Chief and a member of the Steering Committee of IEEE JOURNAL OF EMERGING AND SELECTED TOPICS IN POWER ELECTRONICS. He is an Associate Editor of IEEE TRANSACTIONS ON INDUSTRY APPLICATIONS.